Appendix E – Detailed Reply to Peer Review Comment #22

On the Relevance of Multiple Fracture Initiation-Arrest-Reinitiation Events to the Behavior of Nuclear Reactor Pressure Vessels

Dr. B. Richard Bass
Oak Ridge National Laboratory
Oak Ridge, TN 37831 USA

Dr. Claud E. Pugh
ORSA, Inc.
Knoxville, TN 37922 USA

June 14, 2004

Helmut Schulz's Comment #22:

For the fracture mechanics approach being used the status of validation/verification is well demonstrated for crack initiation and limited stable or unstable crack extension. Although present safety standards or codes do allow the application of crack arrest for multiple initiating events in principle, the supporting experiments are very limited. Furthermore, to the knowledge of the reviewer analysis being performed on such tests (for example NKS test at the MPA Stuttgart) were not able to predict consistently re-initiation and multiple arrest conditions. To evaluate the need to address this issue more deeply, it would be helpful to know if multiple initiation and arrest conditions are really connected to the scenarios being investigated or are only treated as theoretical possibility.

Basic Reply by Staff of Oak Ridge National Laboratory (ORNL)

Given that a flaw may exist within the wall of nuclear reactor pressure vessel (RPV), it is consistent with U.S. experimental evidence and analytical fracture-mechanics predictions that the flaw can propagate into the RPV wall by multiple cleavage run-arrest events when the RPV is exposed to hypothetical pressurized thermal-shock (PTS) loads. Information supporting this view is given in the following pages.

Supporting Information from ORNL Staff

1. Background

Since the late 1960s, the Heavy-Section Steel Technology (HSST) program at ORNL has conducted integrated experimental and analytical studies of the behavior of RPVs in support of the U.S. nuclear safety endeavors. [In 1974, the U.S. Nuclear Regulatory Commission (NRC) was created and charged with regulatory authority to ensure safety within the U.S. nuclear enterprise. The HSST work has been part of the NRC's safety research studies since that time.] The primary purposes of the HSST program have been to: (1) develop a detailed understanding of the fracture behavior of thick-sections of RPV steels

over range of conditions prototypical of RPV applications, (2) establish fracture methods (fracture models and associated computer codes) suitable for representing that behavior, and (3) perform and analyze large-scale fracture experiments to validate the applicability of the methods to prototypical RPV conditions. The studies have examined, in technically progressive phases, fracture initiation (brittle and ductile), arrest, re-initiation, mode interaction, environmental effects (e.g., radiation effects), and many associated features (e.g., effects of limited constraint, flaw shape and size, specimen size, multiaxial loads, cladding, weldments, and time-temperature histories). The experiments have employed RPV plate, forging, weldments, and cladding materials.

The two sets of HSST large-scale experiments that have most clearly involved multiple fracture initiation-arrest events have been the thermal-shock experiments (TSEs) of thick cylinders and the nonisothermal wide-plate experiments (WPEs). For purposes of the present discussion, it is felt that the TSEs provide the best vehicle for demonstrating (1) the feasibility of multiple run-arrest fracture events occurring in thick cylindrical sections exposed to thermal transients and (2) the ability of the fracture mechanics models used in the NRC's PTS reevaluation project to predict such behavior. Specifically, applicability of the fracture methodology embodied in the computer program FAVOR (v.03.1) (Dickson 01a, 01b) is the focus here.

The reader is referred to (Pugh 88) and (Bass 86) for information concerning the WPE test series. While the sixteen WPEs experienced multiple run-arrest events, the dynamic nature of those tests does not lend them to providing the easy and obvious argument needed here. The conditions of the WPEs were such that dynamic analyses were needed to adequately model them. The large mass and stiffness of the TSE specimens and also of RPVs eliminates dynamic effects from fracture considerations in those cases.

2. Thermal-Shock Experiments (TSEs)

2.1 Overview of TSE Program

During the 1970s and early 1980s, the HSST program performed a series of 12 fracture experiments using large-scale (1-m diameter) pressure vessels under steady pressure and temperature conditions. Those experiments were called Intermediate Vessel Tests (ITVs), and they are individually discussed in ORNL reports (Bryan 75, 78a, 78b, 79, 85, 87a, 87b). When the ITV test series was well underway, the HSST program planned and started a phase of large-scale fracture experiments using thick cylinders and thermal-shock loads. This series of eight thermal-shock experiments (TSEs) was carried out at ORNL from 1975 to 1983 under the leadership of R. D. Cheverton.

(Cheverton 86) gives an extended summary of these experiments and describes that the TSEs were conducted to investigate the behavior of surface cracks in thick cylinders under conditions relevant to those that could be encountered during a large-break LOCA. It was known that injection of cold water by the emergency core cooling system into a hot reactor vessel after a LOCA would produce low temperature and high thermal-stress conditions under which a small flaw might extend. It was also known that the propensity for crack propagation in an operating RPV would depend upon the degree of fracture-toughness degradation due to neutron exposure and the temperature of the cooling water.

When planning the TSE tests, the ORNL team recognized that thermal-shock situations involve features that had not been adequately examined experimentally at that time, e.g., biaxial stresses, steep gradients in stress and toughness through the wall, variations in these parameters with time, crack arrest in a rising K_I field, reinitiation of crack propagation after arrest, and warm prestressing (WPS). While the combined effect of high K_I and low fracture toughness in the inner-surface region could result in flaw propagation, it was also recognized that the positive gradient in the fracture toughness through the vessel wall provides a mechanism for crack arrest. Thus, a shallow flaw was envisaged to hypothetically initiate, propagate

through a distance, arrest, and then reinitiate as the transient time progresses. Consequently, it was expected that deep flaws could result from this type of initiation-arrest scenario and potentially experience multiple initiation and arrest events during a single thermal transient.

As described in (Cheverton 86), ORNL constructed critical-crack-depth curves like that shown in Fig. 1 as an aid in designing and interpreting the TSEs. Such pretest curves were constructed using the OCA-II (see Ball 84) computer code, and posttest analyses used the OCA-P computer code (see Cheverton 84). **These codes were forerunners of the current FAVOR computer code that is being used in the NRC's PTS reevaluation program**.

As an illustration, Fig. 1 shows the predicted behavior of a surface-breaking flaw during a hypothetical transient by plotting the crack depths corresponding to initiation and arrest events ($K_I = K_{Ic}$ and $K_I = K_{Ia}$). Multiple crack run-arrest events are shown in this example computation.

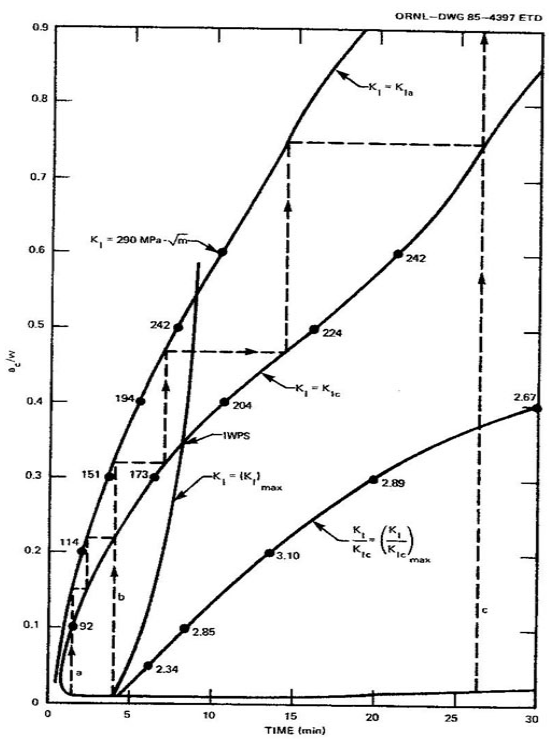

Fig. 1. Critical-crack-depth curves for a PWR vessel during a hypothetical LBLOCA. (a = crack depth and w = wall thickness)

Warm prestressing (WPS) was also recognized to be capable of preventing reinitiation at depths less than the final arrest depth indicated by Fig. 1. The WPS concept means that a flaw will not initiate when K_I is decreasing with time even though K_I may reach or exceed K_{Ic}. Under thermal-shock loading, a deep flaw can conceivably experience its maximum K_I value at a time before the crack-tip temperature has decreased enough to make $K_I \geq K_{Ic}$. During the thermal shock, K_I for a given crack depth increases and then decreases with the temperature gradient. However, K_{Ic} continues to decrease as long as the temperature continues to decrease. The curve in Fig. 1 labeled $K_I = (K_I)_{max}$ shows the times at which K_I reaches a maximum for various crack depths. Thus, for times less than indicated by this curve K_I is always increasing, and for greater times K_I is always decreasing. If WPS is effective, then crack initiation would be limited to times to the left of this curve.

Eight TSE experiments were carried out in two phases that used different specimens and test conditions. The first four TSEs were conducted from September 1975 to January 1977 and used hollow cylindrical specimens fabricated from the trepanned cores taken from the ITV forgings (A508 class-2 steel). These tests are discussed in detail by (Cheverton 76 and 77). The test system used chilled water or water-alcohol mixtures (-23°C) to produce thermal stresses in the heated (288°C) test specimens containing a long internal surface flaw. The test cylinders had an OD of 530 mm (21-in.) and an ID of 240 mm (9.5-in.), and they were 910mm (36-in.) in length. The flaws were shallow with a depth of either 11mm (0.42-in.) or 19 mm (.75-in.). As discussed by (Cheverton 76 and 77), the fracture results from these four experiments were in good agreement with predictions from LEFM analyses which made use of properties values from small laboratory specimens. However, because of the specimen stiffness, deep crack penetrations could not be achieved. Therefore, from August 1979 to May 1983, a second set of four experiments (TSE-5, 5A, 6, and 7) was performed with larger specimens in which deeper crack advances could occur. This second set of four TSEs is addressed in detail in the following pages.

Identification of the Four TSEs that used Large (1-m diam) Specimens

Detailed reports covering the second set of four HSST TSE tests are given by (Cheverton 85a and b), and an overall summary is given in (Cheverton 86). The cylinders used for these tests were made of A508, Class 2 steel, and had an OD of 991mm (39-in.), ID of 682 mm (27-in.), and length of 1220 mm (48-in.). They were given a heat treatment to result in the desired fracture-toughness values. Figure 2a shows a schematic of a TSE test cylinder installed in the ORNL TSE test facility. The test cylinders contained inner-surface flaws and were heated to 96°C prior to being submerged in liquid nitrogen (-196°C) to provide the thermal shock to the inner surface. A specimen and tank schematic are shown in Fig. 2b.

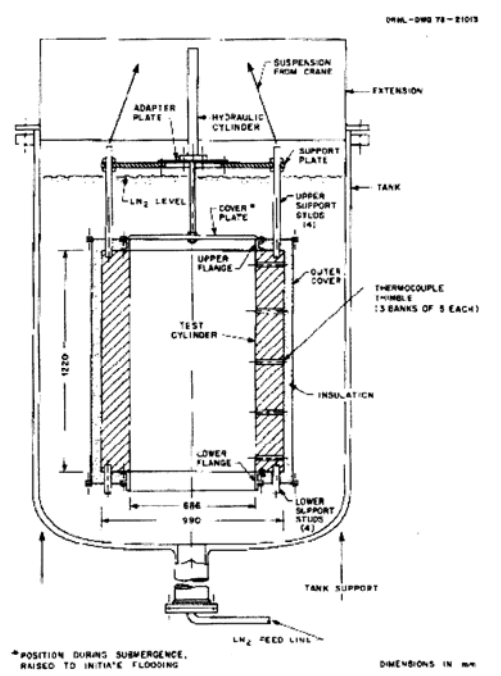

Thermal-shock test cylinder and facility (ORNL, USA).
(ORNL-DWG 78-E1013)

Fig. 2(a). TSE test facility used in TSE-5, 5A, 6, and 7.

Fig. 2(b). Typical TSE test specimen like those used in TSE-5, 5A, 6, and 7.

The test cylinders for TSE-5, 5A, and 6 contained long surface flaws with depths a = 16, 11, and 7.6 mm (0.3-in.), respectively, while the TSE-7 specimen contained a finite length flaw that was 37 mm (1.46-in.) long and 14 mm (0.55-in.) deep. Since the emphasis in this current writing is on multiple crack initiation-arrest-reinitiation events, the following paragraphs address TSE-5, 5A, and 6 where the long flaws propagated into the wall is multiple steps. In TSE-7, the initial flaw extended on the surface in a single event and bifurcated many times to produce an extensive cracking pattern, and therefore this complex situation is excluded from the following discussion. Key observations from experiments TSE-5, 5A, and 6 are given below along with the pretest and posttest analysis results.

2.3. Pretest Analyses of TSE-5, 5A, and 6

In order to further describe the test conditions and results of the pretest analyses that were performed at ORNL, Section 4.2 (*Final Pretest Analysis*) of NUREG/CR-4249 (Cheverton 85a) follows below. The pretest analyses predicted that TSE-5, 5A, and 6 would experience three, four, and one crack initiation-arrest events, respectively. Later in Paragraph 2.4 of this present document, a summary comparison is given of these pretest results, those of posttest analyses, and experimental observations.

The discussion below from (Cheverton 85a) show the critical-crack-depth curves derived from pretest analyses. These curves predicted that TSE-5 would experience three initiation-arrest events, and the final predicted crack depth of a/w = 0.50 to 0.70, depending upon the effectiveness of WPS effects. In the case of TSE-5A, four run-arrest events were predicted with the final a/w ≈ 0.65 (assuming warm prestressing is effective). One fracture initiation event was predicted for TSE-6 with the final a/w ≈ 0.95.

4.2 Final Pretest Analysis

4.2.1 TSE-5

Test conditions assumed for the final pretest analysis of TSE-5 are listed in Table 4.1, and the results of the analysis are presented in Figs. 4.6 and 4.7. Figure 4.6 shows a set of critical-crack-depth curves that indicates the expected behavior of the long axial flaw during TSE-5. It includes the initiation curve ($K_I = K_{Ic}$), the arrest curve ($K_I = K_{Ia}$), the warm prestress curve [$K_I = (K_I)_{max}$], and the maximum K-ratio curve [$K_I/K_{Ic} = (K_I/K_{Ic})_{max}$]. Also included in Fig. 4.6 are temperatures corresponding to several points along the initiation curve and several values of $(K_I/K_{Ic})_{max}$ along the maximum K-ratio curve.

The dashed lines in Fig. 4.6 represent the possible behavior of the flaw during TSE-5, assuming $(a/w)_{initial} = 0.10$. If warm prestressing were not effective and if the crack front remained reasonably uniform in depth (retained its two-dimensional nature), it is apparent that the flaw would penetrate ~90% of the wall. However, if warm prestressing were effective, the maximum penetration might be limited to ~56%. Deeper penetration could result, even with warm prestressing effective, if the dashed curve happened to hit the $K_I = K_{Ic}$ curve just below the point of incipient warm prestressing, in which case the penetration would be ~70%. The least penetration would occur when the dashed line hit the $K_I = K_{Ic}$

Table 4.1. Test conditions for TSE-5 pretest analysis

Test cylinder	TSC-1
Test-cylinder dimensions, m	
Outside diameter	0.991
Inside diameter	0.686
Wall thickness	0.152
Length	1.22
Test-cylinder material	A 508 class-2 chemistry
Test-cylinder heat treatment	Tempered at 613°C for 4 h
K_{Ic} and K_{Ia} curves used in TSE-5 final design analyses	ASME Sect. XI, Appendix A RTNDT = −34°C
Flaw (initial)	Long axial sharp crack, a = 15 mm
Temperatures, °C	
Wall (initial)	93
Sink	−196
Fluid-film heat transfer coefficient	h_f vs T curve based on liquid-nigrogen development studies

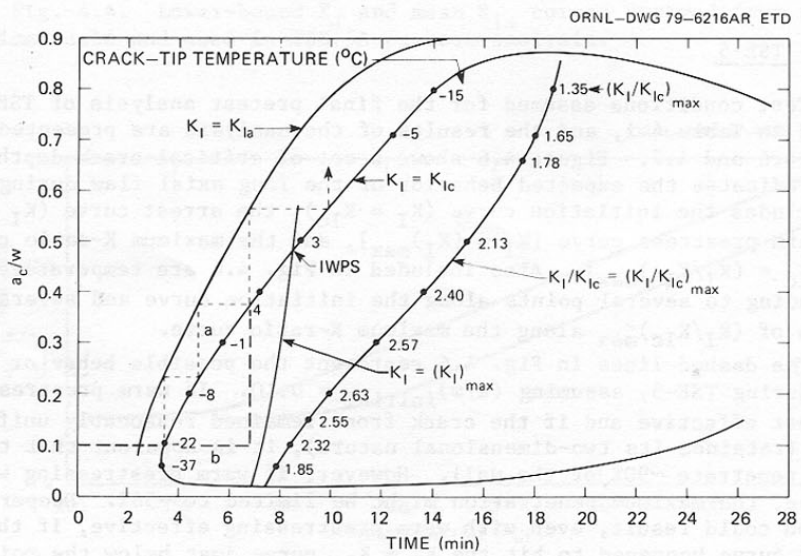

Fig. 4.6. Critical-crack-depth curves for pretest analysis of TSE-5.

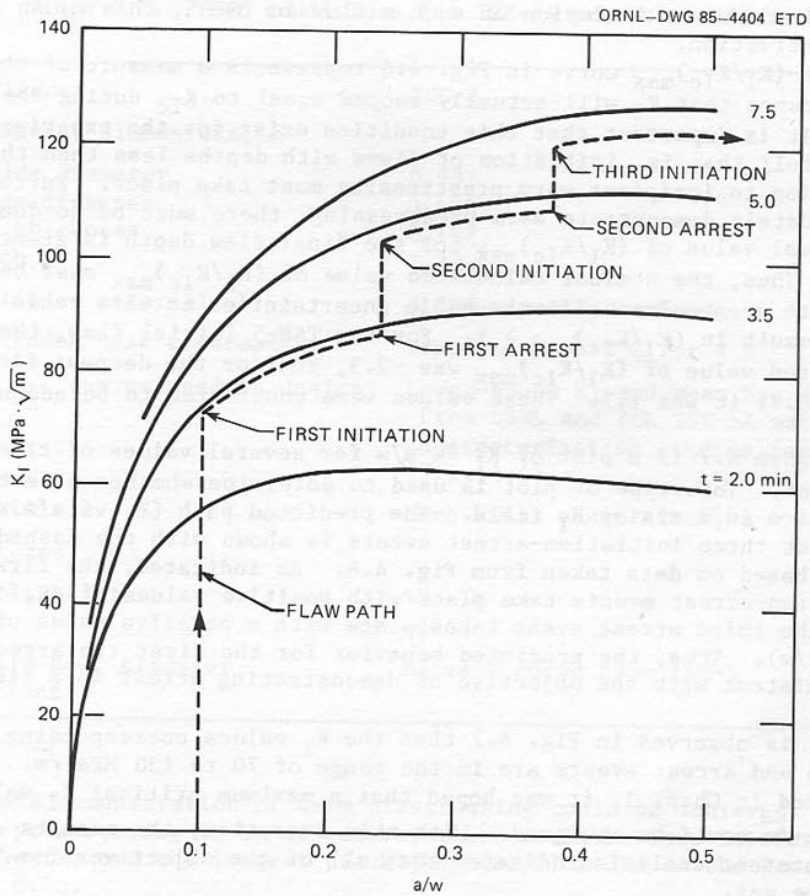

Fig. 4.7. K_I vs a/w for TSE-5 design conditions.

curve just above incipient warm prestressing. For this case the penetration would be limited to ~50%. Thus, the nominal range of predicted final crack depth for TSE-5 was 50 to 70%.

In Fig. 4.6 the area circumscribed by the $K_I = K_{Ic}$ curve and the $K_I = (K_I)_{max}$ curve represents a zone in which flaws with higher-than-anticipated effective toughness could initiate. The result of the higher toughness could be an increase in the crack-jump distance, as illustrated in Fig. 4.6, assuming an initial flaw depth (a/w) of 0.1 and taking the dashed-line path b as opposed to a. In this hypothetical case, crack initiation would be delayed from t = 3.4 min to 6.8 min, and the crack would extend in a single jump from a/w = 0.1 to 0.56 instead of to a/w = 0.23.

It is also of interest to note in Fig. 4.6 that a long crack jump can also be obtained with a very shallow, sharp flaw, that is, with flaw depths represented by the lower portion of the $K_I = K_{Ic}$ curve. Because

of the inadvertent inclusion of such a flaw in TSE-5, this is an important observation.

The $(K_I/K_{Ic})_{max}$ curve in Fig. 4.6 represents a measure of the degree of assurance that K_I will actually become equal to K_{Ic} during the experiment. It is important that this condition exist for the experiment to be successful; that is, initiation of flaws with depths less than that corresponding to incipient warm prestressing must take place. Furthermore, to adequately demonstrate warm prestressing, there must be no doubt that the actual value of $(K_I/K_{Ic})_{max}$ for the final flaw depth is greater than unity. Thus, the nominal calculated value of $(K_I/K_{Ic})_{max}$ must be large enough to accommodate all reasonable uncertainties in this ratio and, thus, result in $(K_I/K_{Ic})_{max} > 1$. For the TSE-5 initial flaw, the nominal calculated value of $(K_I/K_{Ic})_{max}$ was ~2.3, and for the deepest final flaw (a/w = 0.7) it was 1.7. These values were considered to be adequate for TSE-5.

Figure 4.7 is a plot of K_I vs a/w for several values of time in the transient. This type of plot is used to determine whether arrest will take place in a rising K_I field. The predicted path (K_I vs a/w and t) for the first three initiation-arrest events is shown with the dashed lines and is based on data taken from Fig. 4.6. As indicated, the first two initiation-arrest events take place with positive values of $dK_I/d(a/w)$, while the third arrest event takes place with a negative value of $dK_I/d(a/w)$. Thus, the predicted behavior for the first two arrest events is consistent with the objective of demonstrating arrest in a rising K_I field.

It is observed in Fig. 4.7 that the K_I values corresponding to initiation and arrest events are in the range of 70 to 130 MPa$\cdot\sqrt{m}$. As mentioned in Chap. 1, it was hoped that a maximum critical K_I value near 250 MPa$\cdot\sqrt{m}$ could be achieved. With this exception, the results of the final pretest analysis indicated that all of the objectives for TSE-5 could be met.

4.2.2 TSE-5A

Because the scope of TSE-5A was the same as that for TSE-5, the pretest calculated behavior of the long axial flaw for the two experiments was similar. However, there were differences in the assumed thermal transients, toughness curves, and initial flaw depths, and these differences resulted in somewhat different calculated behaviors for the flaws.

Test conditions assumed and/or specified for TSE-5A are shown in Table 4.2 and include a thermal transient equal to that actually achieved during TSE-5 (more severe than used in the TSE-5 pretest analysis), toughness curves based on very extensive material-characterization studies (lower-bound K_J and mean K_{Ia}), and an initial crack depth (a/w) equal to 0.075 as compared with 0.10 for TSE-5.

Results of the final pretest analysis for TSE-5A are shown in Fig. 4.8. As indicated by this set of critical-crack-depth curves, the flaw would penetrate deeper than 90% of the wall without warm prestressing but only 45 to 65% with warm prestressing. The range of $(K_I/K_{Ic})_{max}$ for the latter range of final crack depths is 2.2 to 1.7, and, thus, presumably

Table 4.2. Test conditions for TSE-5A pretest analysis

Test cylinder	TSC-2
Test-cylinder dimensions, m	
Outside diameter	0.991
Inside diameter	0.686
Wall thickness	0.152
Length	1.22
Test-cylinder material	A 508 class-2 chemistry
Test-cylinder heat treatment	Tempered at 679°C for 4 h
K_{Ic} and K_{Ia} curves used in design	Lower-bound K_J and mean K_{Ia} data from ORNL and BCL TSE-5A material-characterization studies (see Fig. 4.4)
Flaw (initial)	Long axial sharp crack, a = 11 mm
Temperatures, °C	
Wall (initial)	93
Sink	−196
Fluid-film heat transfer coefficient	h_f vs T curve from TSE-5

an adequate demonstration of warm prestressing could be achieved. Assuming warm prestressing to be effective, there would be four initiation-arrest events, and the longest crack jump ($\Delta a/w$) would be the last and equal to 0.20.

Figure 4.8 includes a curve referred to as $K_I = (K_I)_{max(a/w)}$, which represents the crack depth for which $dK_I/da = 0$ for different times in the transient. If arrest takes place at a depth less than that corresponding to the $K_I = (K_I)_{max(a/w)}$ curve, it will do so in a rising K_I field. Thus, according to the pretest analysis, the first two arrest events would take place in a rising K_I field.

Another point of interest illustrated in Fig 4.8 is that the K_I values corresponding to initiation and arrest events cover a range from ~70 to 140 MPa•$\sqrt{m}$, that is, the lower to midtransition region. This range is similar to that calculated for some PWR large-break loss-of-coolant accident cases, but the maximum value is still less than desired (250 MPa•$\sqrt{m}$). With this exception, the results of the final pretest analysis indicated that the objectives of TSE-5A could be met.

4.2.3 TSE-6

A long crack jump with arrest deep in the wall was specified for TSE-6. To achieve this without the initial flaw having to be very shallow or blunted, it was necessary to use a thinner wall (76 mm) for TSE-6

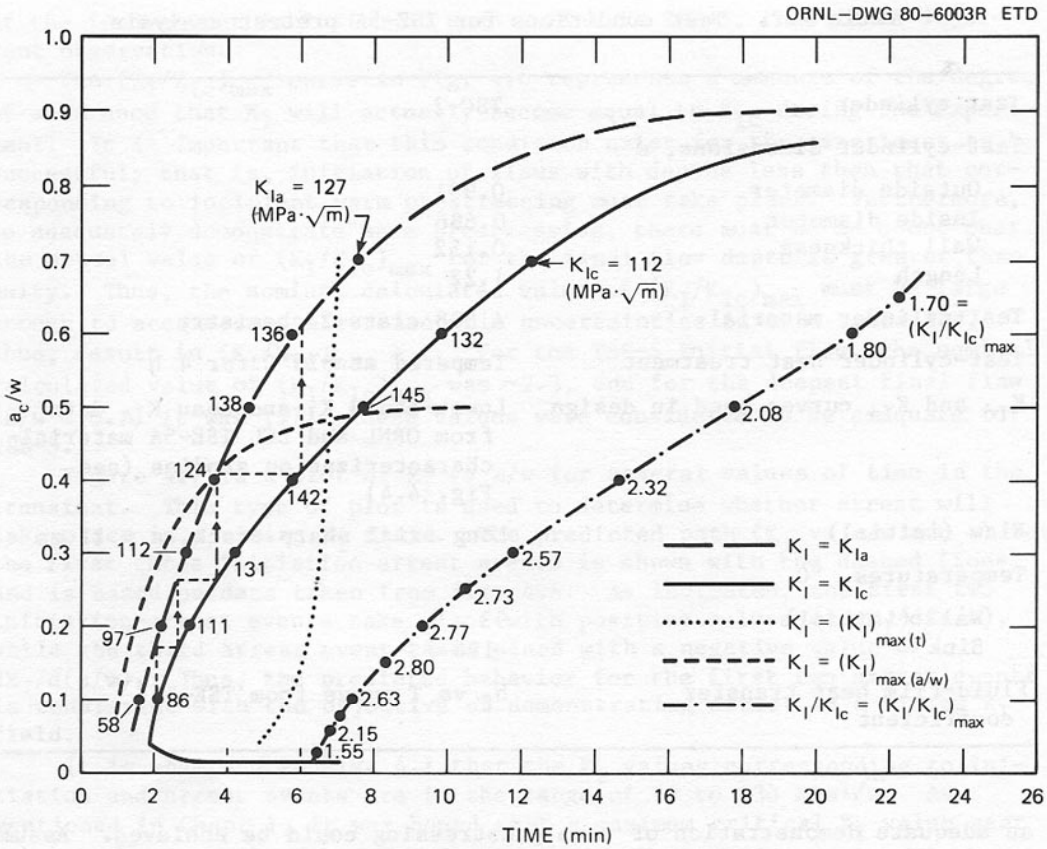

Fig. 4.8. Pretest critical-crack-depth curves for TSE-5A assuming TSE-5 thermal transient and TSE-5A lower-bound K_{IJ} and mean K_{Ia} curves.

than that used for the TSE-5 and TSE-5A test cylinders (152 mm) and to use the same low fracture-toughness properties actually obtained for the TSE-5 test cylinder (see Table 4.3 for test conditions used in pretest analysis). This combination resulted in a set of calculated critical-crack-depth curves with nearly vertical sections of the initiation and arrest curves (Fig. 4.9). The dashed lines in Fig. 4.9 represent the expected behavior of the flaw and indicate a single long crack jump from a/w = 0.1 (initial flaw) to a/w = 0.95. Reinitiation would not be likely because of warm prestressing or $(K_I/K_{Ic})_{max} < 1$. For the initial flaw, $(K_I/K_{Ic})_{wps} = 1.36$, which was large enough to ensure initiation prior to warm prestressing. Furthermore, K_I values all along the initiation and arrest curves were below upper-shelf toughness values.

The expected inability of the flaw to completely penetrate the wall under thermal-shock loading conditions only is illustrated in Fig. 4.10,

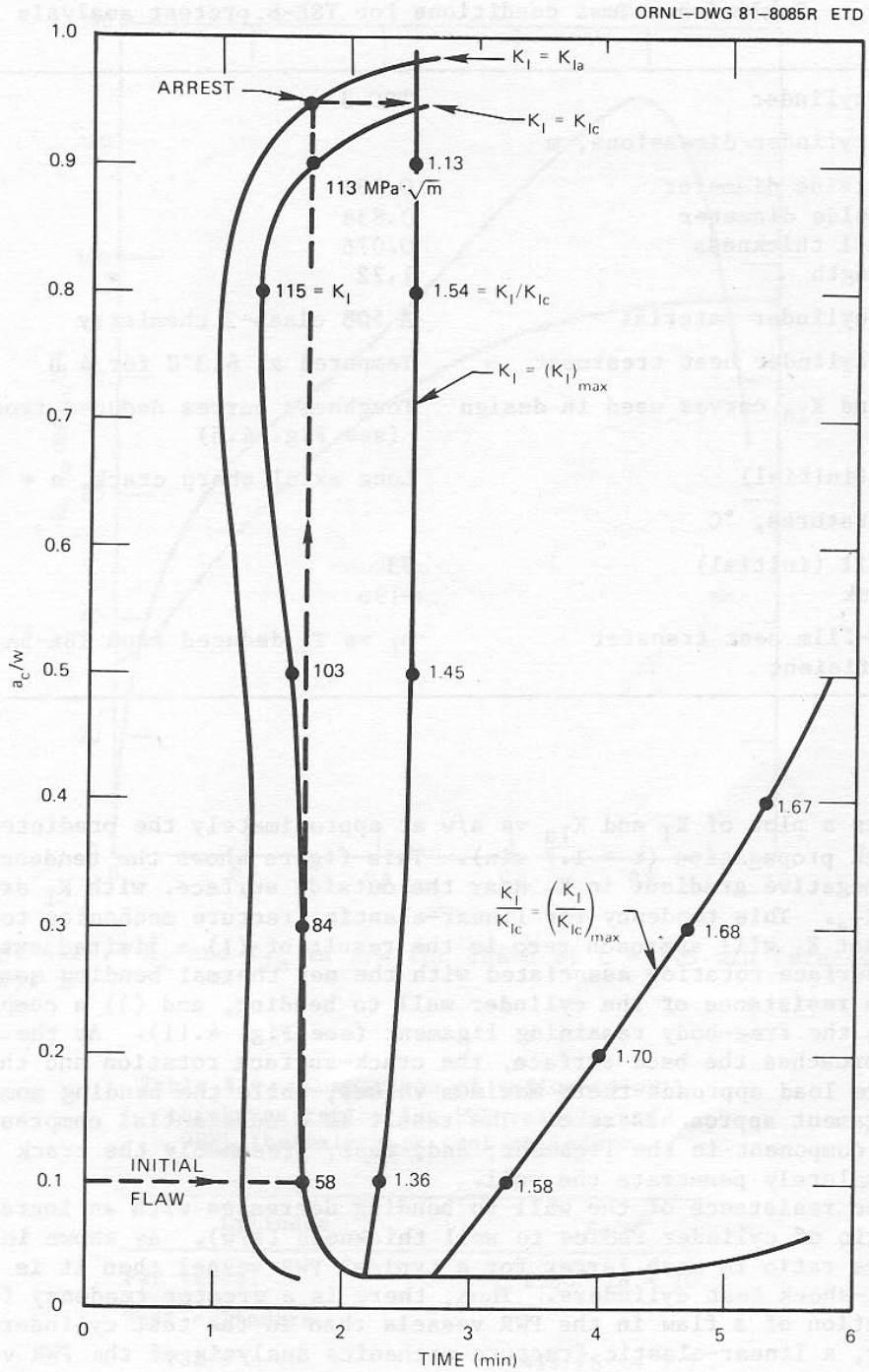

Fig. 4.9. Pretest critical-crack-depth curves for TSE-6.

Table 4.3. Test conditions for TSE-6 pretest analysis

Test cylinder	TSC-3
Test-cylinder dimensions, m	
Outside diameter	0.991
Inside diameter	0.838
Wall thickness	0.076
Length	1.22
Test-cylinder material	A 508 class-2 chemistry
Test-cylinder heat treatment	Tempered at 613°C for 4 h
K_{Ic} and K_{Ia} curves used in design	Toughness curves deduced from TSE-5 (see Fig. 4.5)
Flaw (initial)	Long axial sharp crack, a = 7.6 mm
Temperatures, °C	
Wall (initial)	93
Sink	−196
Fluid-film heat transfer coefficient	h_f vs T_s deduced from TSE-5A

which is a plot of K_I and K_{Ia} vs a/w at approximately the predicted time of crack propagation ($t \approx 1.7$ min). This figure shows the tendency for a steep negative gradient in K_I near the outside surface, with K_I dropping below K_{Ia}. This tendency for linear-elastic fracture mechanics to predict that K_I will approach zero is the result of (1) a limited extent of crack-surface rotation associated with the net thermal bending moment, (2) the resistance of the cylinder wall to bending, and (3) a compressive load on the free-body remaining ligament (see Fig. 4.11). As the crack tip approaches the back surface, the crack-surface rotation and the compressive load approach their maximum values, while the bending moment at the ligament approaches zero. The result is a substantial compressive-stress component in the ligament, and, thus, presumably the crack could not completely penetrate the wall.

The resistance of the wall to bending decreases with an increase in the ratio of cylinder radius to wall thickness (r/w). As shown in Table 4.4, the ratio is much larger for a typical PWR vessel than it is for the thermal-shock test cylinders. Thus, there is a greater tendency for deep propagation of a flaw in the PWR vessels than in the test cylinders. However, a linear-elastic fracture-mechanics analysis of the PWR vessel indicates that for this case, too, a long axial flaw could not fully penetrate the wall under thermal-shock loading only (see Chap. 1). Thus, if during TSE-6 the flaw did not breach the wall, this would be considered an adequate demonstration.

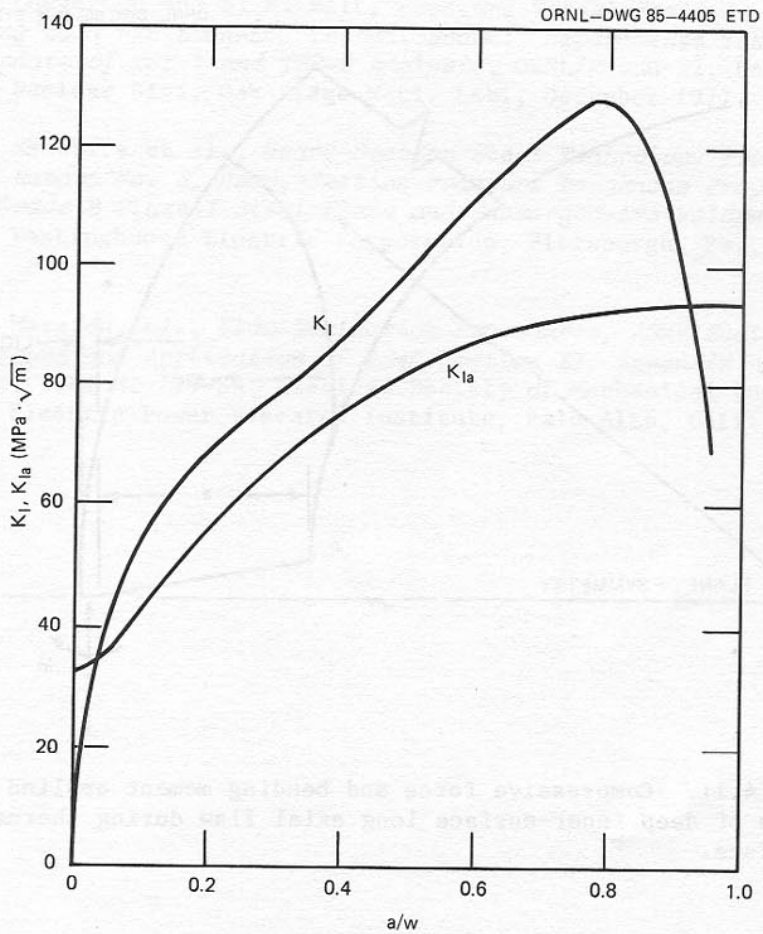

Fig. 4.10. K_I and K_{Ia} vs a/w for TSE-6 at t = 1.5 min (pretest analysis).

Table 4.4. Comparison of radius-to-wall thickness ratios for PWR vessels and ORNL thermal-shock test cylinders

Cylinder	r_i/w[a]
PWR vessel	2180/216 = 10
Test cylinders	
TSE-6	419/76 = 5.5
TSE-5, TSE-5A	346/152 = 2.3
TSE-1, TSE-2, TSE-3, TSE-4	114/152 = 0.8

[a]Inside radius (r_i)/wall thickness (w), dimensions in millimeters.

2.4. Observations from Tests TSE-5, 5A, and 6

2.4.1. TSE-5

TSE-5 experienced three initiation/arrest events with deep penetration of the two dimensional flaw. The following pages are taken from Chapter 8 of NUREG/CR-4249 (Cheverton 85a) and address the test results and critical crack-depth curves generated posttest. The posttest analyses used improved fracture-toughness models and actual temperature transients. While the pretest analyses predicted the correct number of initiation-arrest events, the posttest analyses provided improved results.

8.3 Crack Depths

Estimates of crack depth prior to the test and at the time of each of the three events were obtained from three UT transducers secured to the outer surface of the test cylinder directly opposite the tip of the flaw. Once the test was completed and the outer-surface insulation was removed, UT instrumentation was used to obtain a detailed description of the final crack depth. Finally, a pie-shaped section of the cylinder wall containing the primary flaw was removed from the cylinder and was cut into several lengths to expose cross sections of the flaw at several positions along the length of the cylinder (Fig. 8.9). Once the cross sections were examined, the fracture in each block was completed under mechanical loading conditions at cryogenic temperatures to reveal the fracture surfaces. The cross sections and fracture surfaces revealed the initial crack depth, first crack-arrest depth, and final crack depth, but the second arrested crack depth was not discernible. A typical cross section and fracture surface are shown in Figs. 8.10 and 8.11, and all depth measurements are shown in Fig. 8.12.

The data in Fig. 8.12 show good agreement between crack-depth measurements and indicate that crack penetration in the central portion of

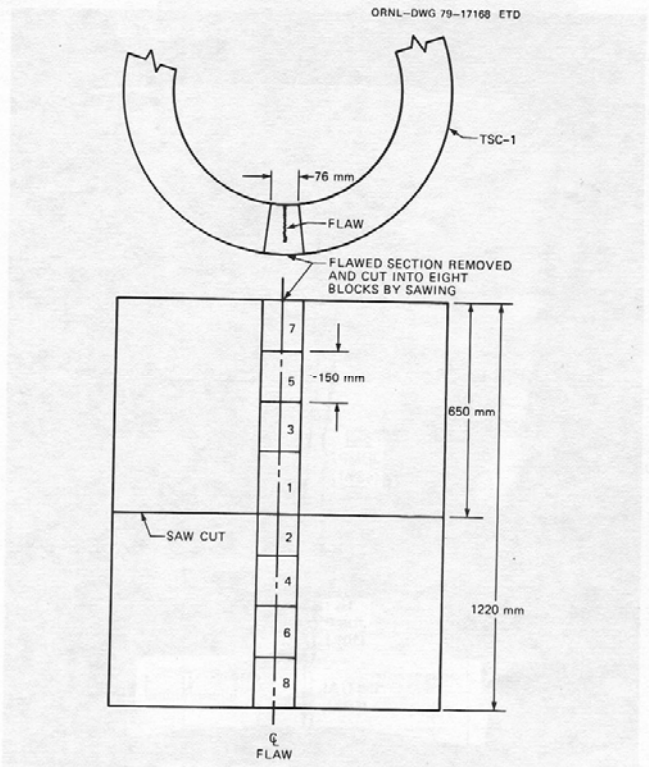

Fig. 8.9. Section of TSE-5 test cylinder removed for study of crack profile and fracture surfaces.

M&C PHOTO Y164626

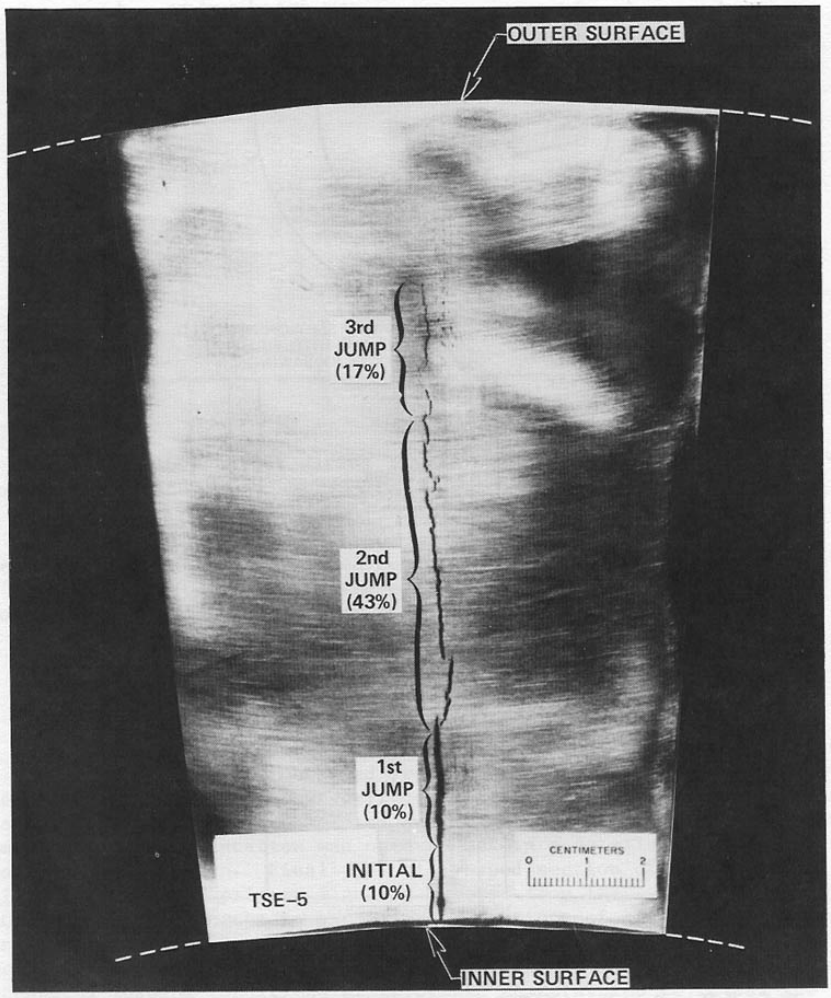

Fig. 8.10. Cross section of TSE-5 final flaw near midlength of test cylinder.

8.4 Fracture-Mechanics Analysis of Primary Flaw

8.4.1 Posttest analysis based on design toughness curve

The TSE-5 pretest fracture-mechanics analysis indicated that three initiation-arrest events would take place during TSE-5, and indeed that is what happened. However, a comparison of the estimated and actual times for the events shows that the latter times were significantly earlier due in part to the greater severity of the actual thermal shock. Thus, before additional comparisons could be made, it was necessary to conduct a posttest fracture-mechanics analysis using the measured temperature distributions. The corresponding critical-crack-depth curves, assuming that the TSE-5-design K_{Ic} vs temperature curve was appropriate, are shown in Fig. 8.13. Superimposed on these curves is the "actual"

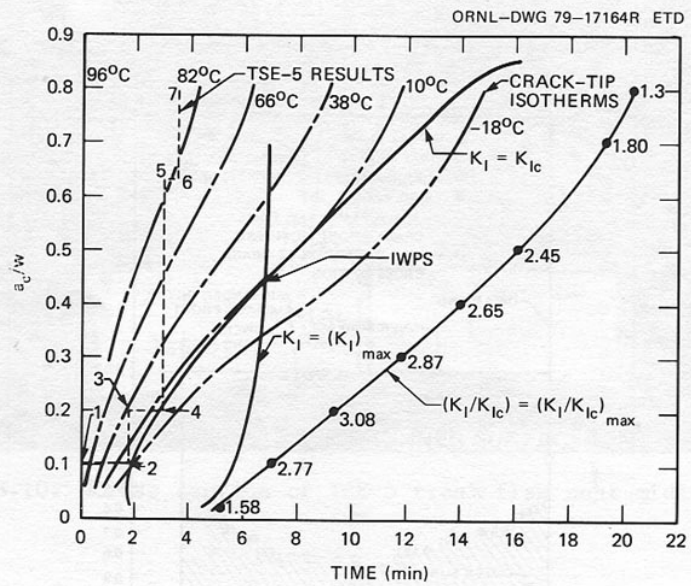

Fig. 8.13. Critical-crack-depth curves from posttest analysis of TSE-5 (original K_{Ic} data).

path of events, using the measured midlength crack-arrest depths. As indicated, the first two initiation events agree well with the calculations, but the very long second crack jump [$\Delta(a/w) \cong 0.4$] resulted in arrest at a much greater depth and temperature than expected. Thus, the toughness at the higher temperature had to be much less than indicated by the design-toughness curve.

8.4.2 K_{Ic} and K_{Ia} values deduced from TSE-5

The calculated K_I vs time and K_I vs a/w curves for the actual thermal shock are shown in Figs. 8.14 and 8.15 with the initiation-arrest events superimposed. As indicated in these figures, the K_I values corresponding to the three initiation-arrest events are 79, 111, and 115 MPa•$\sqrt{m}$ for the initiation events and 86, 104, and 92 MPa•$\sqrt{m}$ for the arrest events. Corresponding temperatures obtained from Figs. 8.1–8.3 are –9, –3, and 79°C for the initiation events and 36, 82, and 89°C for the arrest events. All of these data are summarized in Table 8.1.

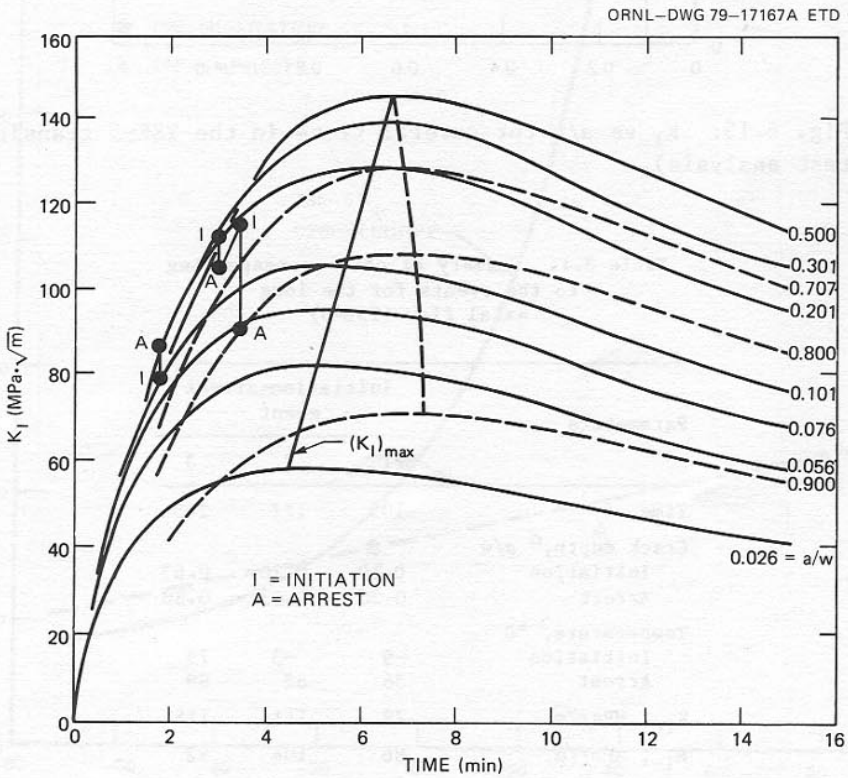

Fig. 8.14. K_I vs time for several crack depths (TSE-5 posttest analysis).

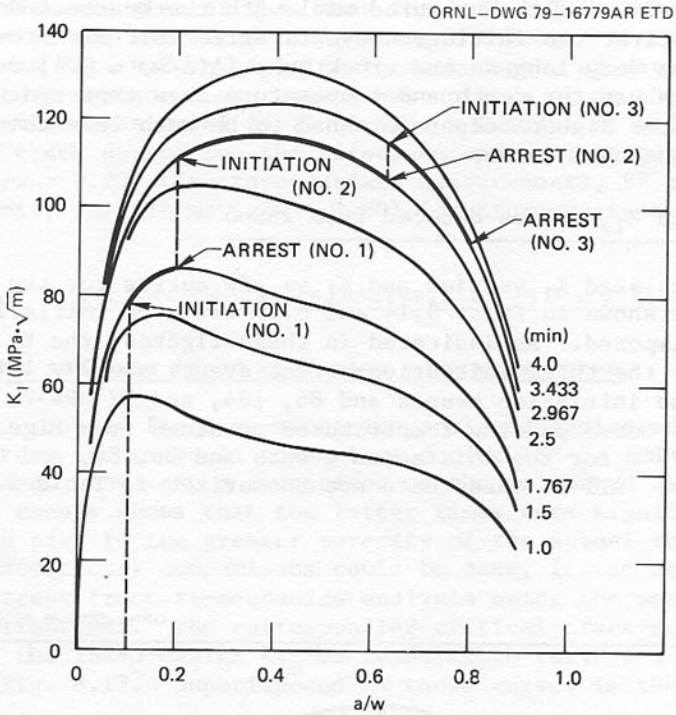

Fig. 8.15. K_I vs a/w for several times in the TSE-5 transient (posttest analysis).

Table 8.1. Summary of data corresponding to the events for the long axial flaw (TSE-5)

Parameters	Initiation-arrest event		
	1	2	3
Time, s	105	177	205
Crack depth,[a] a/w			
Initiation	0.10	0.20	0.63
Arrest	0.20	0.63	0.80
Temperature, °C			
Initiation	−9	−3	79
Arrest	36	82	89
K_{Ic}, MPa·√m	79	111	115
K_{Ia}, MPa·√m	86	104	92
Duration of experiment, min	30		

[a]Maximum depth (midlength of test cylinder).

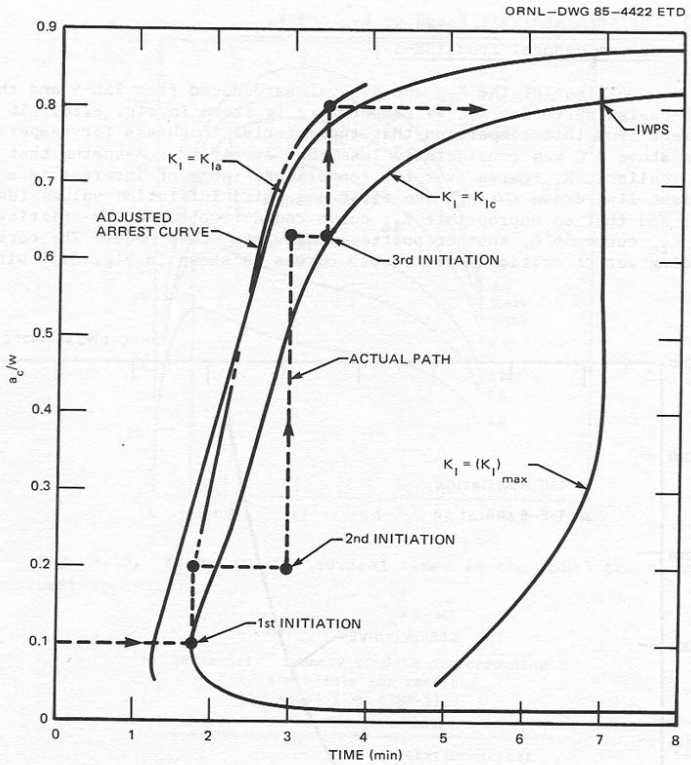

Fig. 8.17. Critical-crack-depth curves from posttest analysis of TSE-5 using TSE-5 K_{Ic} data.

Table 8.2 Crack depths derived from COD data and from direct measurements

Time (s)	Fractional crack depth (a/w)	
	Direct	COD
106	0.10[a]	0.12
106	0.20[a]	0.21
178	0.20[a]	0.22
178	0.63[b]	0.55
206	0.63[b]	0.55
206	0.80[a]	0.72

[a]Fracture-surface measurement.

[b]UT measurement.

In summary, posttest analysis predictions, posttest crack-depth measurements from the fracture surface, and cross-section photo results show good agreement. In conclusion, the LEFM analyses predicted well the nature and magnitude of the multiple-event fracture behavior of TSE-5 under thermal shock loads.

2.4.2. TSE-5A

As discussed on page 34 of (Cheverton 85a), TSE-5A had the same scope as TSE-5, but different thermal transients, fracture toughness, and initial crack-depth made the expected response different for the two experiments. Accordingly, TSE-5A experienced four initiation/arrest events with 50% penetration of the wall, whereas TSE-5 experienced three initiation/arrest events as discussed in the previous paragraphs. A fifth event was prevented by WPS effects, and one of the arrest events took place with K_I increasing with crack depth. After the WPS intervention, the K_I/K_{Ic} ratio reached a maximum value of 2.3 without crack initiation taking place. As was the case for TSE-5, the behavior was consistent in nature with the pretest analyses based on LEFM methods.

The following pages from (Cheverton 85a) discuss the observed crack propagation events and the results of posttest analyses. The posttest analyses here were made using the OCA-P computer code, the best interpretation of actual test specimen material properties and the actual thermal transient. The posttest analyses produce very good predictions of what was observed from test measurements. (Note: When considering Table 9.1 below, it should be kept in mind that the specimen wall thickness was 152 mm. Using this with the crack depth values shown in that table allows calculation of a/w values for ease of comparison with a/w values reported in Table 9.2.)